ISSN 1023-1935, Russian Journal of Electrochemistry, 2009, Vol. 45, No. 9, pp. 1027–1036. © Pleiades Publishing, Ltd. 2009.
Original Russian Text © Yu.G. Chirkov, V.I. Rostokin, 2009, published in Elektrokhimiya, 2009, Vol. 45, No. 9, pp. 1102–1112.

Fuel Cell Oxygen Cathode with Nafion and Platinum: the Effect of Active Layer Heating on Overall Cathode Characteristics

Yu. G. Chirkov[a, z] and V. I. Rostokin[b]

[a]*Frumkin Institute of Physical Chemistry and Electrochemistry, Russian Academy of Sciences, Leninskii pr. 31, Moscow, 119991 Russia*

[b]*Moscow Institute of Engineering Physics, Kashirskoe sh. 31, Moscow, 115409 Russia*

Received April 7, 2008

Abstract—A fuel cell with Nafion and platinum is considered. The effect of heating of the oxygen cathode active layer on the cathode overall characteristics (current and power density) is taken into account for the first time. Attention is focused on calculations of Tafel plots of oxygen cathodes and also on how the active layer temperature changes with the potential. Calculation parameters are as follows: fuel cell initial temperature, cathode active layer thickness, gas-diffusion layer effective heat conductivity and thickness. The following conditions of cathode operation are studied: (1) heat formed in the cathode active layer is almost completely removed, no active layer heating is observed, the active-layer temperature remains equal to that of fuel cell operation; (2) heat removal is impeded, the heat conductivity of the gas-diffusion layer is insufficiently high to remove heat. In the latter case, the active layer temperature may increase by several tens of degrees. A fundamental difference of Tafel plots for the catalytic layers studied in model experiments and the cathodic active layers is demonstrated. In the latter case, the first Tafel plot segment may extend further up to potentials of ~0.6 V.

Key words: fuel cell with Nafion and platinum, oxygen cathode, computer simulation of current generation in cathode, cathodic active layer heating, cathodic Tafel plots

DOI: 10.1134/S1023193509090079

INTRODUCTION

Fuel cells with solid polymeric electrolytes (first of all, Nafion) are considered as the most promising sources of environmentally clean and highly efficient energy in the XXI century. In these electrochemical devices, the most problematic part is the cathode where oxygen is reduced in an acidic medium. The kinetics of this process is rather sluggish. This is why such a large number of studies both experimental and theoretical were devoted to the mechanism of operation of Nafion-platinum cathodes.

Model experiments with equally accessible (in the absence of Ohmic and diffusion limitations) thin catalytic layers (rotating disk electrode and similar methods) allow one to comprehensively study the kinetics of electrochemical processes. Particularly, it was found [1–11] and repeatedly confirmed that for the oxygen reduction on Pt in acidic media, two Tafel-plot slopes are observed, namely, 60 mV (high potential range) and 120 mV (low potential range). However, this seemingly established viewpoint was called into question by the authors of [12] and considered as an artifact.

In [12], a system of parameters was proposed that allows one to characterize Tafel plots of oxygen reduction on Pt in the cathodes of Nafion fuel cells in the high potential range. Attention was focused on the fact that in many studies [12–18] carried out on such cathodes in a wide range of practically important potentials up to 0.6 V, only one Tafel plot was observed with a slope close to 60 mV, especially at elevated temperatures and pressures. At the same time, in model experiments with Pt, the low-slope range came extended to ~0.8 V.

We do not dwell into details of the scientific discussion aroused by [12]. We pursue a different goal, namely, to demonstrate that the aforementioned contradiction and the artifact are illusory and that on an equally accessible Pt surface, the Tafel plot of oxygen reduction in acidic media always has two regions, namely, 60 and 120 mV. However, for Nafion–Pt fuel cell cathodes, a more complicated set of Tafel slopes can be observed in the E vs. $\log I$ coordinates (E is the electrode potential, I is its net current). Moreover, the earlier ignored factors may be responsible for these "distortions".

[z] Corresponding author: olga.nedelina@gmail.com (Yu.G. Chirkov).

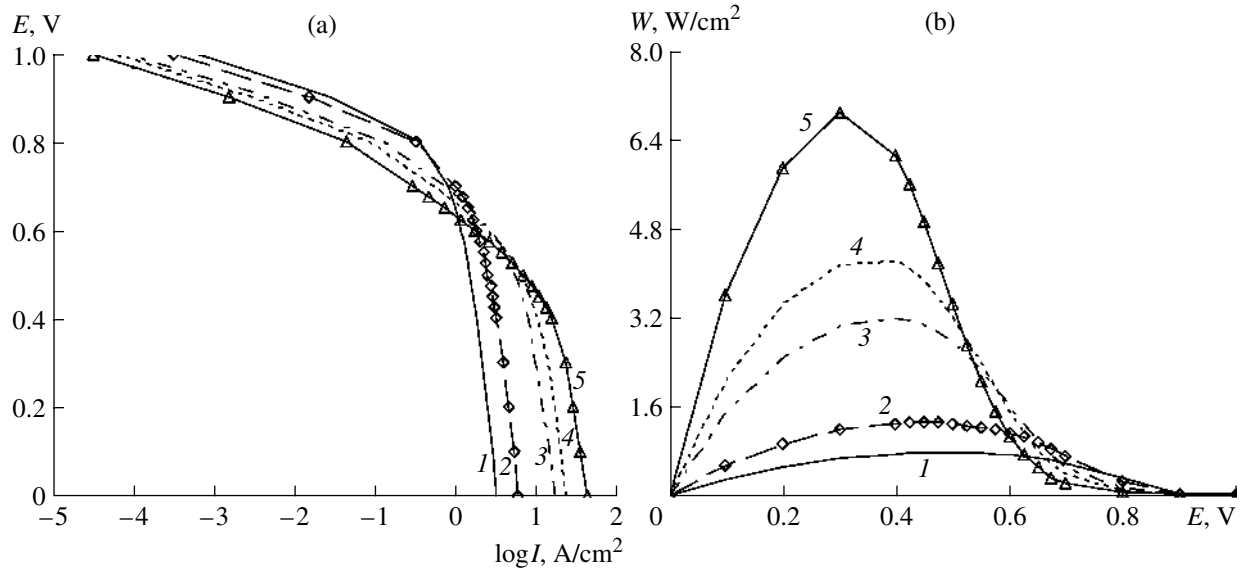

Fig. 1. Oxygen cathode of a fuel cell with Nafion and platinum: (a) Tafel plots and (b) dependences of the power density on the cathodic potential. t = 80°C, p^* = 101 kPa. Δ, μm: (*1*) 20, (*2*) 10, (*3*) 3, (*4*) 2, (*5*) 1.

TAFEL PLOTS OF CATHODIC ACTIVE LAYER

First of all, note that Tafel slopes of 60 and 120 mV were obtained in [1–11] when studying the catalytic layers with the internal surface *equally accessible for electrochemical reaction*. On the other hand, cathodic active layers are always *unequally accessible* to a certain degree, and some limitations arise for an electrochemical process in the active layer. Hence, first of all, it is expedient to calculate Tafel plots of the cathodic active layers containing Nafion and Pt and then compare their features with the Tafel plots for equally accessible catalytic layers (model experiments). This can be performed by computer simulation of the active layer structure for a cathode with a solid polymeric electrolyte, using the techniques developed in a series of studies [19]. Our calculations were carried out using equations derived in [20].

Let us choose the parameters involved in these equations. They are clearly divided into the following groups:

(1) *external conditions of fuel cell operation*: fuel cell temperature, cathodic gas chamber (bipolar plate) pressure, active layer thickness;

(2) *electrochemical process of oxygen reduction on smooth platinum*: cathodic steady-state potential, Tafel plot breakpoint potential, Tafel slopes in the high and low potential ranges, characteristic bulk current density;

(3) *active-layer structure parameters*: bulk concentrations of Nafion, carrier (with Pt), and voids; average diameter of pores in carrier grains and grain porosity; catalyst specific surface and its fraction involved in the electrochemical process;

(4) *coefficients that characterize the mass and electricity transfer*: effective diffusion coefficient of oxygen and effective specific proton conductivity in the cathodic active layer, oxygen solubility in Nafion.

The characteristics of an oxygen cathode with Nafion and Pt, employed in our calculations are collected in Table 6 in the end of this paper. Figure 1 shows the results of calculations of Tafel plots for an oxygen cathode of a fuel cell with Nafion and Pt at temperature t = 80°C and pressure p^*= 101 kPa.

Figure 1a shows the corresponding Tafel plots in coordinates E vs. $\log I$ for the active layer thickness Δ of 20, 10, 3, 2, and 1 μm. Figure 1b shows the electric power density W generated in the oxygen cathode as a function of potential. Tafel plots in Fig. 1a have two segments with pronounced slopes and the transient region between them. The nature of these three regions should be commented.

According to [21], for a fuel cell cathode with a solid polymeric electrolyte at a fixed potential E, the dependence of the net current I on the active layer thickness has an extremum. The overall current has a maximum at a certain thickness $\Delta = \Delta^*$ optimal for current generation. Table 1 shows the results of calculations of Δ^* and the corresponding optimal (maximum) net currents I^* and optimal power densities W^* for the conditions same as those taken in plotting curves in Fig. 1.

Net current values shown in Table 1 are the maximum possible values attainable for the cathode at a given fixed potential (and at certain other parameters characterizing the active layer, Table 6). To reach these currents, the active layer thickness should be equal to the optimal thickness $\Delta = \Delta^*$. For example, for net current $I \sim 4.3$ A/cm^2 to be reached at a potential E = 0.55 V, the active layer thickness should be reduced to $\Delta^* \sim 2$ μm. As follows from Table 1, as the cathodic potential drops from its

steady-state value E_{st}, the optimal thickness decreases from several hundred μm to several tenth of μm. Moreover, the maximum possible net cathodic current increases from several hundredth to several tens of A/cm^2, and the power W^* at potential $E = 0.3$ reaches a value $W^* = 14.2$ W/cm^2.

Now, we compare the data in Table 1 (optimal values) with the data in Fig. 1 (real values for a cathode with a fixed active layer thickness). In Fig. 1a, all E vs. $\log I$ curves in the high potential range ($E_{st} \geq E \geq E^*$) have one and the same slope of 60 mV. This is associated with the fact that, here, the layer is equally accessible for the electrochemical process, because the active layer thicknesses Δ in curves *1–5* in Fig. 1a (from 1 to 20 μm) are much lower that the corresponding optimal thicknesses Δ* (several hundred μm, data of Table 1). This is why, here the current generation occurs in the kinetic mode and the net current $I \sim \exp[2.3(E_{st} - E)/0.06]$.

In terms of study [20], in the "transition potential range" ($E^* \geq E \geq E^{**}$; E^* is the breakpoint potential in the Tafel plot observed at fulfillment of the condition on equal accessibility of the catalytic layer to the current generation process, the meaning of potential E^{**} will become clear below), the active layer part localized closer to the Nafion membrane generates current corresponding to the slope of 120 mV, while its remaining part generates current corresponding to 60 mV. In the "transition potential range", the Ohmic and diffusion limitations operate starting from a cathode potential E at which the active layer thickness Δ becomes equal to its optimal value Δ* (data of Table 1). Figure 1a (compare curves *1* and *5*) shows that the *transition potential range* shortens with an increase in the cathode active layer thickness.

As the potential decreases further, a moment comes inevitably (here, $E = E^{**}$) when the electrochemical kinetics is described by a Tafel curve with a slope of 120 mV (*low potential range* in terms of study [20]). In contrast to hydrophobized cathodes with liquid electrolytes, for cathodes with Nafion it is typical that in the low potential range, the net current increases in proportion with $\sim \exp[\eta_0/2]$, where η_0 is the cathodic overpotential, i.e., for $E \leq E^{**}$ the net current $I \sim \exp[\{2.3(E_{st} - E)/0.12\}/2]$ [22]. Hence, in Fig. 1a, all curves in the range of sufficiently low potentials have one and the same slope equal to 240 in place of 120 mV. Thus, for this cathode, the Tafel plots (with slopes of 60 and 240 mV) differ from the plots of thin active layers with equally accessible catalyst surface (in this case, the slopes are 60 and 120 mV).

It deserves mention once again how the shape of Tafel plots of porous cathodes varies with the active layer thickness (Fig. 1a). The whole range of cathodic potential variations can be conditionally divided into two parts, namely, above 0.5 V and below 0.5 V. As the thickness Δ decreases in the high potential range ($E > 0.5$ V), the net current becomes progressively smaller as follows from Fig. 1b and, the other way round, in the low potential range ($E < 0.5$ V), the current increases with a decrease in Δ. As a result of this, for very thin active layers (several μm, curves *3–5* in Fig. 1a), it can be assumed at a certain stretch that the first segment in the Tafel plot of a porous electrode that gradually passes to the progressively flattening "transition potential region" extends to the range of lower potentials instead of coming to end as soon as at $E^* \sim 0.825$ V (curves *1* and *2* in Fig. 1a, "thick" active layers). This trend manifests itself to the greater extent in curve *5*, Fig. 1a (Δ = 1 μm, very "thin" active layer).

Table 1. Dependence of optimal values of net current and power density on the cathodic potential

E, V	I^*, A/cm^2	Δ*, μm	W^*, W/cm^2
1.0	8×10^{-3}	600	8×10^{-3}
0.9	0.06	100	0.05
0.8	0.37	17.9	0.29
0.7	1.01	8.33	0.71
0.65	1.64	5.14	1.06
0.6	2.65	3.19	1.59
0.55	4.28	1.97	2.36
0.5	6.93	1.21	3.46
0.4	18.1	0.46	7.25
0.3	47.4	0.18	14.2

Thus, we have arrived to an important conclusion that when one deals with cathodes with very thin active layers, the effects mentioned in [12] inevitably arise. However, this is not the only reason for possible elongation of the first segment in Tafel plots for cathodes with Nafion and Pt to reach approximately 0.6 V. The other factors that can operate in the same direction should also be discussed.

MODELING OF CATHODE ACTIVE LAYER HEATING PROCESSES

Fuel cells with Nafion and Pt demonstrate very high overall characteristics (their power density exceeds 1 W/cm^2) as compared with fuel cells of other types. These characteristics continue to grow with the transition to thin catalytic layers of enhanced activity. Quite recently, the optimum loading was considered to correspond to carrier (carbon black)–Pt with $g_w = 20$ wt % [23]. Since that time, the latter characteristic increased to $g_w = 60$–70 wt %. A considerable increase in the specific surface of carbon carrier grains allowed the specific surface of Pt particles on the carrier to be increased up to values of nearly $S^* = 100$ m^2/g Pt [12]. The degree of Pt utilization (the fraction of platinum surface involved in the electrochemical process) increased from the conventional values of 20–25% to those record-breaking of 75–98% [24, 25]. This in aggregate favors the further increase in the power density of fuel cells with Nafion. However, simultaneously, the

Table 2. Dependence of exchange current on temperature (for oxygen reduction on Pt in the fuel cell cathode active layer with Nafion)

T, °C	20	50	80	110	140	170	200
i_0, A/cm^2	6.14×10^{-10}	1.0×10^{-8}	1.01×10^{-7}	7.15×10^{-7}	3.8×10^{-6}	1.61×10^{-5}	5.68×10^{-5}

amount of heat liberated in fuel cells increases. Heat should be removed, which is often associated with difficulties unobserved in those cases where the fuel cell power density was still low and the cathodic active layer was only several tens μm thick.

In a cathodic active layer, the active mass is always heated, which inevitably increases the exchange current. In [26], the temperature dependence of the exchange current for oxygen reduction was characterized as follows:

$$i_0 = i_0^{\text{ref}} \exp[8804(1/T_{\text{ref}} - 1/T)]. \quad (1)$$

Assume that at 50°C ($T_{\text{ref}} = 323$ K), the exchange current for platinum $i_0^{\text{ref}} = 10^{-8}$ A/cm^2 [27]. Table 2 shows exchange currents calculated using Eq. (1) in the temperature range from 20 to 200°C. It becomes clear that as the temperature increases in this interval, the exchange current increases by 5 orders of magnitude. Thus, heating of the cathodic active layer and its operation at elevated temperatures may considerably affect the exchange current value i_0 and, hence, the characteristic bulk current i^* (data of Table 6) and further the cathodic net current I.

Heat formed in the cathodic active layer escapes to the outer space mostly through the gas-diffusion layer. Figure 2 schematically illustrates the fuel cell cathode with solid polymeric electrolyte and its surrounding parts. Designations in Fig. 2: M is a Nafion membrane, AL is the cathodic active layer, GDL is the gas-diffusion layer, BP is the bipolar plate (gas chamber).

Several dozens of studies were devoted to calculations of nonisothermal models of fuel cells with solid polymeric electrolytes. The first publications appeared in 1993 [28, 29]. Later, scientists returned many times to the problem of temperature and heat flow distribution in a fuel cell with Nafion (e.g., see [30–32]).

If the heat conductivity of a gas-diffusion layer is insufficiently high, then as the current generated in the cathode increases, the active layer temperature can considerably increase which, in turn, favors an additional increase in the net current. This process continues until the active layer temperature reaches a certain equilibrium value T^* for which the flow of heat generated in the cathode becomes equal to the flow of heat removed through the gas-diffusion layer, i.e., the flow that is, apparently, proportional to the temperature difference $T^* - T$, where T is the temperature of fuel cell operation.

To access the effect of cathode heating on the magnitude and nature of its overall characteristics, the following assumptions are drawn that simplify the calculations.

1. Assume that no heat exchange occurs between the membrane and the active layer so that the heat liberated in the cathodic active layer is removed only towards the gas-diffusion layer. This assumption doesn't seem rather strained. As was shown by calculations of the heat flow distribution in a fuel cell with Nafion [30–32],

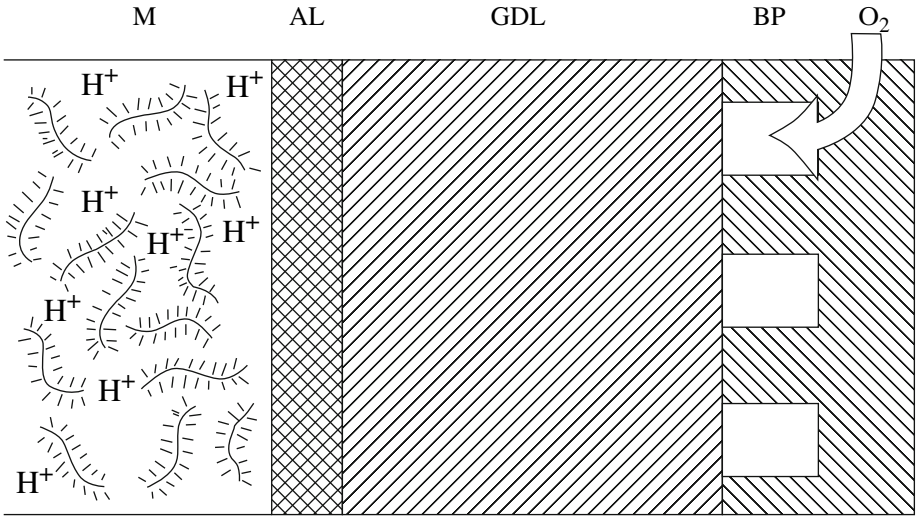

Fig. 2. Fuel cell cathode with solid polymeric electrolyte. M is Nafion membrane, AL is cathodic active layer, GDL gas-diffusion layer, BP is bipolar plate.

for approximately equal degrees of wetting of gases with saturated vapor on the anode and the cathode, the temperature profile of a fuel cell looks as an isosceles trapezoid and the thermal flows in the Nafion membrane can be assumed to be negligible. Moreover, the weakness of heat flows in the membrane is due to the fact of all heat liberated by a fuel cell only 10% [33] accounts for Joulean heat associated with the finite resistances for different components used in a fuel cell. Thus, there arises a remarkable opportunity to study the heat exchange of a seemingly "isolated" cathode without considering the other parts of a fuel cell with Nafion.

2. Insofar as the active layer thickness (from several tens μm to even several μm) is much smaller than the gas-diffusion layer thickness (several hundred μm), we will assume in our calculations that the equilibrium temperature in the active layer is constant throughout the thickness and equal to T^*.

3. We assume that the temperature at the interface of the gas-diffusion layer with the bipolar membrane is T, i.e., the temperature of fuel cell operation.

4. The thermal characteristics of the gas-diffusion layer are assumed uniform throughout its thickness so that the heat transfer in it is characterized by the coordinate-independent effective heat conductivity.

5. The efficiency of current generation in the cathode is assumed constant and independent of the cathodic potential.

Then, the condition of equality of thermal flows generated in the cathode active layer and removed through the gas-diffusion layer is written as

$$(1-\varepsilon)I(\Delta, T^*)E = \lambda^*(T^* - T)/100\delta. \qquad (2)$$

In this equality, ε is the efficiency of current generation in a fuel cell, $I(\Delta, T^*)$ is the net current on cathode (its value is determined by the active layer thickness Δ and equilibrium temperature T^*), E is the cathode potential, λ^* is the effective heat conductivity of the gas-diffusion layer, δ is the gas-diffusion layer thickness.

The simplest analysis of Eq. (2) is as follows. If λ^* the effective heat conductivity of the gas-diffusion layer is infinitely large, then, due to the finiteness of the product in the left part of Eq. (2), the difference $(T^* - T) = 0$. Thus, no heating of the cathodic active layer occurs, because heat liberated in the active layer is removed without difficulty through the gas-diffusion layer. Another limiting case takes place when parameter λ^* is small. Let λ^* tend to zero, then, it is evident that the active layer temperature T^* should tend to ∞. The gas-diffusion layer fails to sustain the heat transfer and, according to calculations, powerful heating of the active layer takes places and its temperature can increase by tens of degrees.

One of the goals of specific calculations below is to find out what is meant under the words "high" and "low" heat conductivity of the gas-diffusion layer. For which λ^* values, the heating can be neglected or, the other way round, should attract the keenest attention.

Table 3. Heat conductivity of different substances at t = 80°C and pressure p^* = 101 kPa

Substances	Heat conductivity (W/mK)
Hydrogen	0.206
Oxygen	0.0307
Nitrogen	0.0295
Air	0.03
Water (vapor)	0.0246
Water (liquid)	0.67

OVERALL CATHODIC CHARACTERISTICS THAT TAKE INTO ACCOUNT THE HEATING PHENOMENON

Equality (2) allows one to determine the equilibrium values of T^* and I for the given cathodic potential E and parameters T, Δ, ε, λ^*, δ by varying the temperature T^* and the net current I (this current is calculated using equations shown in [20]; the temperature-dependent exchange current involved in these equations is determined using Eq. (1)).

These equilibrium values are sought by means of a simple procedure. A certain arbitrary value of T^* is taken and the active-layer net current is calculated for this temperature. The resulting I and T^* values are substituted into equality (2). If the left part of Eq. (2) turns out to exceed its right part, this means that the gas-diffusion layer does not provide the necessary removal of heat so that the initially chosen value T^* is not equal to the sought equilibrium temperature of the active layer. Now, it is necessary to slightly change the T^* value and repeat the net-current calculations followed by the procedure of comparison of quantities in Eq. (2). Thus, using the method of successive approximations, these procedures should be repeated until the left and right parts in Eq. (2) become equal to one another. This will provide us with the true values of I and T^*.

It remains to decide which values of parameters will be used in calculations. Table 6 shows the list of all parameter of the cathodic active layer and the gas-diffusion layer. Throughout the further calculations, it is assumed that ε = const = 60% in Eq. (2). Thus, 40% of energy produced in the fuel cell is converted to heat. It is also assumed that the gas-diffusion layer thickness always δ = 400 μm and the gas pressure in the bipolar plate p^*= 101 kPa.

It is evident that the gas-diffusion layer should have high porosity, up to 80%. On the other hand, according to the data of [34] shown in Table 3, the heat conductivity of gases is low. Hence, it should be expected that the effective heat conductivity should amount to tenth fractions of W/mK.

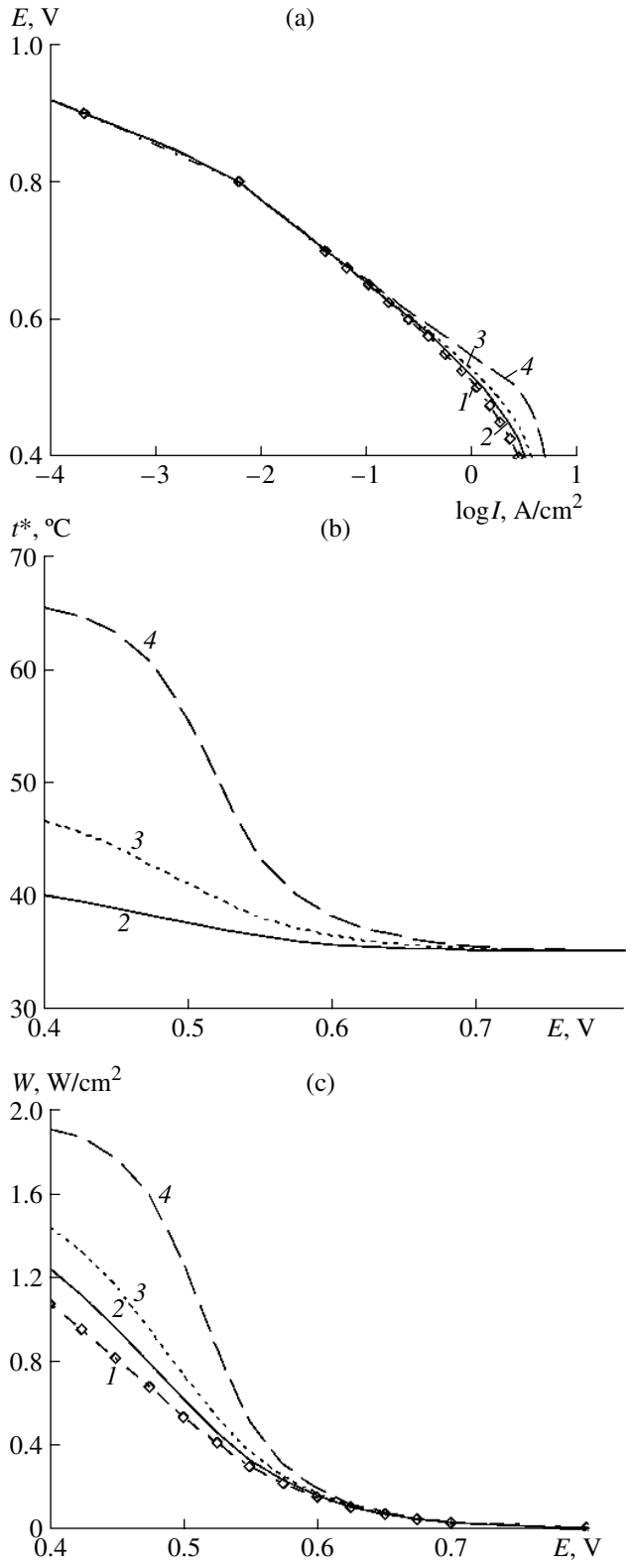

Fig. 3. Fuel cell oxygen cathode with Nafion and platinum: (a) Tafel plots, (b) extent of active layer heating, and (c) power density vs. cathodic potential. t = 35°C, p^* = 101 kPa, Δ = 5 μm, δ = 400 μm. λ^*, W/mK: (*1*) absence of active layer heating ($\lambda^* = \infty$), (*2*) 0.4, (*3*) 0.2, (*4*) 0.1.

The value of λ^* was experimentally assessed in [31, 32, 35, 36]. In [31], λ^* = 0.3 W/mK (Quintech™ carbon paper) was shown. In [32], the effect of fluoroplastic on the effective heat conductivity of the gas-diffusion layer was studied. It was shown that λ^* = 0.48 W/mK and 0.22 W/mK in the absence and in the presence of fluoroplastic (20 wt %), respectively. In [35], the effective heat conductivity of an E-TEK GDL was shown to be λ^* = 0.2 W/mK. Thus, the order of magnitude of λ^* is indeed tenth fractions of W/mK. In further calculations, we assume that the effective heat conductivity of the gas-diffusion layer fits the range $0.1 \le \lambda^* \le 0.4$ W/mK.

Now we show the results of calculations. Figure 3 demonstrates the characteristics of an oxygen cathode of a fuel cell with Nafion and Pt. These are the following three characteristics: (a) Tafel plots obtained by taking into account the possible heating of the active layer, (b) the degree of active layer heating characterized by the dependence of its equilibrium absolute temperature t^* on the potential, and (c) the dependence of the power density on the potential. The fuel cell temperature t = 35°C (T = 308 K), the active layer thickness Δ = 5 μm. The effective heat conductivity of the gas-diffusion layer took several values, namely, λ^*, W/mK: (curve *1*) in the absence of active layer heating (formally, $\lambda^* = \infty$), (*2*) 0.4, (*3*) 0.2, (*4*) 0.1.

Figure 3 shows that the effective heat conductivity λ^* = 0.4 can be assumed to be virtually infinitely high, because curve *2* in Fig. 3a differs only slightly from curve *1*. Then, as λ^* decreases, the Tafel plots gradually become straighter. Figure 3b shows that the cathodic active layer heating increases from its initial temperature t = 35°C with the decrease in the effective heat conductivity of the gas-diffusion layer. For λ^* = 0.1, the ability of the gas-diffusion layer to remove heat considerably weakens, and the active layer temperature increases by 30 degrees. In Fig. 3c, the cathode power density is shown to increase with the decrease in the cathodic potential and λ^*.

Let us consider the data shown in Fig. 4. They corresponds to the fuel cell temperature higher than that in Fig. 3, namely, t = 60°C (T = 333 K). It is evident that with an increase in the fuel cell temperature, the degree of heating also increases by 40 degrees for λ^* = 0.1 (curve *4* in Fig. 4b); the power density values also increase (Fig. 4c).

Figure 3a clearly shows that at a potential E = 0.825 V, the first Tafel slope passes to the "transition potential range" (this is also observed for the Tafel plot with t = 60°C); hence, up to potentials E ~ 0.5–0.6 V, the Tafel plot can be characterized by a single slope close to 60 mV only with certain reservations.

Yet another important factor should be stressed. Let us show that in practice, the Tafel slope that begins in the "high potential range" can be extended below 0.825 V only for cathodes with sufficiently thin active layers. Figure 5 shows the results of calculations of Tafel plots of

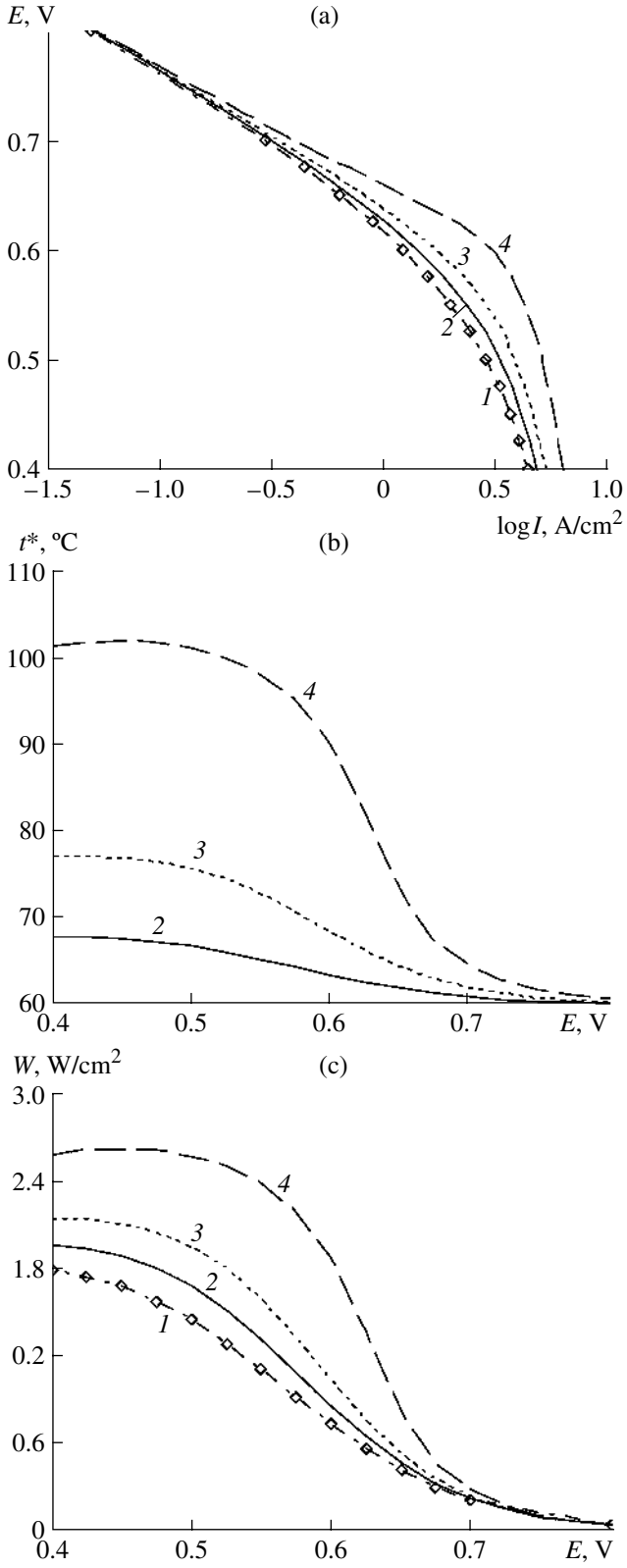

Fig. 4. Fuel cell oxygen cathode with Nafion and platinum: (a) Tafel plots, (b) extent of active layer heating, and (c) power density vs.cathodic potential. t = 60°C, p^* = 101 kPa, Δ = 5 μm, δ = 400 μm. λ*, W/mK: (*1*) absence of active layer heating (λ* = ∞), (*2*) 0.4, (*3*) 0.2, (*4*) 0.1.

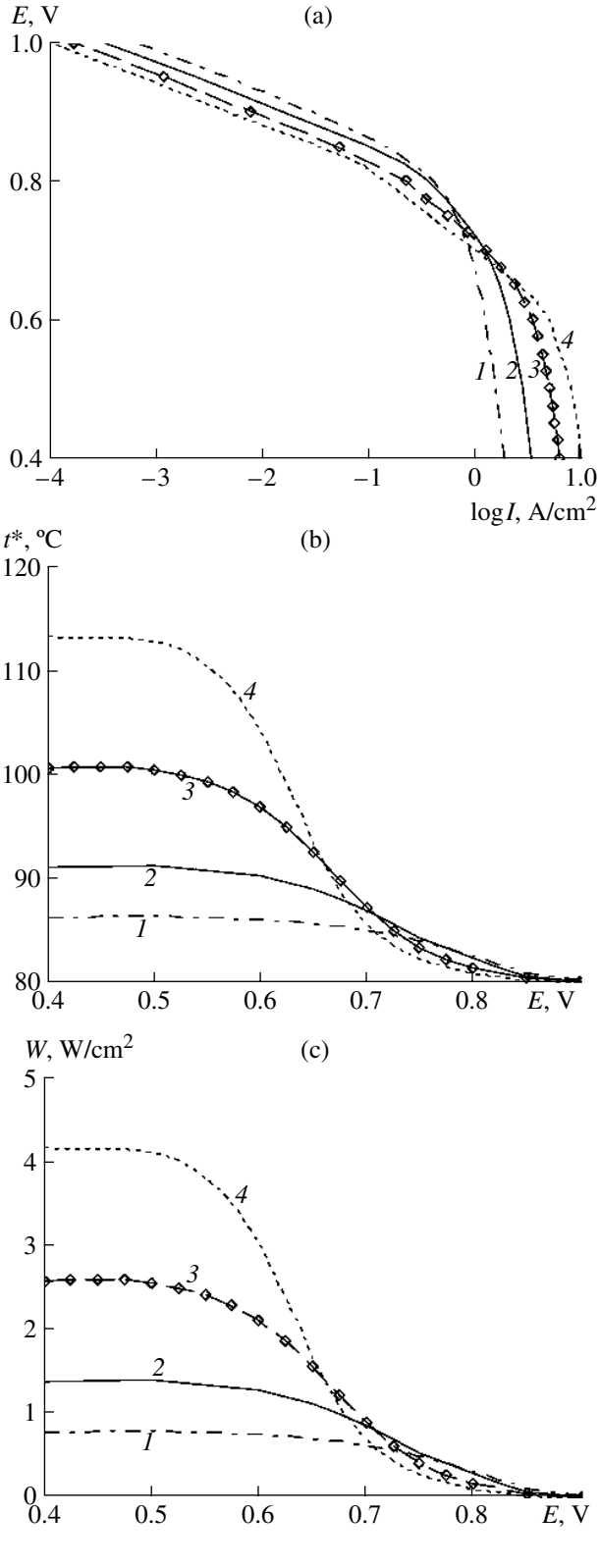

Fig. 5. Fuel cell oxygen cathode with Nafion and platinum: (a) Tafel plots, (b) extent of active layer heating, and (c) power density vs.cathodic potential. t = 80°C, p^* = 101 kPa, λ* = 0.2 W/mK, δ = 400 μm. Δ, μm: (*1*) 20, (*2*) 10, (*3*) 5, (*4*) 3.

Table 4. Dependence of overall characteristics of an oxygen cathode on the potential and active layer thickness. The active layer heating is absent. The fuel cell working temperature $t = 80°C$, gas pressure in a bipolar plate $p^* = 101$ kPa

E, V	Δ^*, μm	I, A/cm^2	W, W/cm^2
0.7	20	0.81	0.57
	10	1.00	0.70
	3	0.73	0.51
0.6	20	1.19	0.71
	10	1.86	1.11
	3	2.65	1.59
0.5	20	1.51	0.76
	10	2.56	1.28
	3	5.51	2.75

Table 5. Dependence of overall characteristics of an oxygen cathode on the potential and the active layer thickness. Active layer heating is present: $\lambda^* = 0.2$ W/mK, $\delta = 400$ μm. Fuel cell working temperature $t = 80°C$, gas pressure in bipolar plate $p^* = 101$ kPa

E, V	Δ, μm	I, A/cm^2	W, W/cm^2	t^*, °C
0.7	20	0.89	0.62	85.0
	10	1.22	0.85	86.8
	3	1.00	0.70	85.6
0.6	20	1.26	0.76	86.0
	10	2.13	1.28	90.2
	3	5.04	3.02	104.2
0.5	20	1.59	0.79	86.4
	10	2.82	1.41	91.3
	3	8.21	4.10	112.8

oxygen cathodes with Nafion and platinum that operate at $t = 80°C$ and have heat conductivity $\lambda^* = 0.2$ W/mK. In this case, the active layer thickness varies from 3 and 5 μm ("thin" active layers) to 10 and 20 μm ("thick" active layers).

Figure 5a shows that one can speak of "extension of the high-potential range" up to $E \sim 0.6$ V only for "thin" active layers (curves *3–4* in Fig. 5a), whereas this effect is absent for "thick" active layers (curves *1–2* in Fig. 5a). Moreover, the thinner active layer the longer the first segment in the Tafel plot.

Indeed, it is only for cathodes with "thin" active layers that the Ohmic and diffusion limitations remain small at potentials below 0.825 V and do not yet manifest themselves to the full extend. Moreover, it is only the cathodes with very thin active layers [37] that allow one to obtain the high net current and power density values (curves *3–4* in Figs. 5a and 5c). Hence, it is not surprising that precisely these cathodes demonstrated the pronounced heating of the active layer, namely, by several tens of degrees (Fig. 5b).

Summarizing, it is expedient to carry out a numerical comparison of the major overall characteristics of a fuel cell cathode with Nafion for those cases where the active layer heating is absent (Fig. 1) or present (Fig. 5). Tables 4 and 5 show the dependences of overall characteristics of an oxygen cathode on the potential and active-layer thickness for these two cases.

Naturally, as the cathode potential decreases (the overpotential increases), the overall characteristics (the current and the power density) tend to increase. However, in the high potential range ($E > 0.7$ V), the characteristics of cathodes with "thick" active layers (20 and 10 μm) exceed those of cathodes with "thin" active layers ($\Delta = 3$ μm). At potentials $E \le 0.6$ V, the situation is reversed, namely, "thin" active layers show advantages in the current generation. This is explained by the fact that the diffusion and Ohmic limitations in active layers rapidly increase as the cathode potential drops (overpotential increases). For $E \ge 0.7$ V, these limitations are low and it is "thick" active layers that are favorable for current generation. However, the current growth in them considerably slows down at $E \le 0.6$ V where the characteristic diffusion and Ohmic lengths become small, namely, about 1 μm.

A comparison of data shown in Tables 4 and 5 also demonstrates the effect of the cathode active layer heating. The temperature grows in parallel with the cathode potential drop. The temperature difference between the active layer and the bipolar plate (temperature of fuel cell operation) $t^* - t$, deg: from 5 to 6.8 at $E = 0.7$ V, from 6 to 24.2 at $E = 0.6$ V, and from 6.4 to 32.8 at $E = 0.5$ V. With the increase in the active layer temperature, the net current on the cathode increases. The latter is observed most clearly for a cathode with a "thin" active layer ($\Delta = 3$ μm).

Finally, going back to the beginning of this paper, to the discussion aroused by study [12], it should be stressed once more that it is unreasonable to look for any experimental errors or any ignored factors in studies [1–11] that have already become classical and use this as the basis for explaining the deviations between the results of these papers and those of studies [12–18]. For the cathodes with a sufficiently thin active layer, one can observe the appearance of high net currents and, as a consequence, the pronounced effect of heating. In such cathodes, the first Tafel segment has the first slope of ~60 mV up to the potential of ~0.6 V.

CONCLUSION

When analyzing the oxygen reduction on Pt in acidic media, it is necessary to distinguish the catalytic layers of a mixture of Nafion and Pt with the surface *equally accessible* for electrochemical processes (model experiments) from the active layers containing

Table 6. Designations for parameters characterizing the active layer, the gas-diffusion layer, and the bipolar plate of a fuel cell cathode with Nafion and platinum and their values taken in calculations

ACTIVE LAYER

External parameters

t = 35, 60 and 80°C are fuel cell temperature

p^* = 101 kPa is the pressure in the gas chamber (bipolar plate) of cathode

Δ = 1, 2, 3, 5, 10, 20 μm are active layer thicknesses

Kinetic parameters of oxygen electroreduction on platinum

E_{st} = 1.05 V is steady-state potential of cathode

E^* = 0.825 V is the breakpoint potential in Tafel plot

$b_1 = (6 \times 10^{-2}/2.3)$ V $= 2.6 \times 10^{-2}$ V is the Tafel plot slope in the high potential range

$b_2 = (12 \times 10^{-2}/2.3)$ V $= 5.2 \times 10^{-2}$ V is the Tafel plot slope in the low potential range

n = 4 is the number of electrons involved in the electrochemical reaction

$F = 9.6 \times 10^4$ C/mol is the Faraday number

i_0, A/cm^2: 2.65×10^{-9}, 2.27×10^{-8}, 1.01×10^{-7} are the exchange currents in the high potential range at temperatures t = 35, 60 and 80°C, respectively

i^*, A/cm^3: 2.73×10^{-3}, 2.34×10^{-2}, 1.04×10^{-1} are characteristic bulk current densities in the high potential range for t = 35, 60 and 80°C, respectively

Parameters of optimal active layer structure

g_e = 0.475 is the bulk concentration of Nafion grains

g_s = 0.525 is the bulk concentration of carrier grains

g_0 = 0 is the bulk concentration of grains-voids

g_w = 60 wt % is the platinum content in carrier grains

d_s = 30 nm is the average diameter of pores in carrier grains

$S^* = 1.03 \times 10^6$ cm^{-1} is the specific surface of catalyst (platinum) for S^{**} = 86 m^2/g Pt

η = 90% is the catalyst surface fraction involved in the electrochemical process

ν = 0.5 is the carrier grain porosity

ρ_p = 21.5 g/cm^3 is the catalyst (platinum) density

ρ_c = 1.8 g/cm^3 is the carrier (carbon black) density

Parameters determining the processes of mass and charge transition

$D_{kn} = 4 \times 10^{-3}$ cm^2/s is the Knudsen diffusion coefficient for gas in carrier grain pores

$D^* = 5.49 \times 10^{-4}$ cm^2/s is the effective diffusion coefficient of oxygen in the active layer

$c_o = 5 \times 10^{-6}$ g-mol/cm^3 is the oxygen solubility in Nafion at p^* = 101 kPa

$k = 1 \times 10^{-1}$ S^{-1} cm^{-1} is the specific conductivity of optimally wetted Nafion

$k^* = 8.37 \times 10^{-3}$ S^{-1} cm^{-1} is the effective specific conductivity of optimally wetted Nafion

GAS-DIFFUSION LAYER

T^* is the equilibrium absolute temperature of the cathodic active layer

λ^* is the effective heat conductivity of the gas-diffusion layer, it varies in the range from 0.4 to 0.1 W/mK

δ = 400 μm is the gas-diffusion layer thickness

ε = 60% is the efficiency of cathode operation in a fuel cell

BIPOLAR PLATE

T = 308, 333 and 353 K is the absolute temperature of fuel cell operation (temperature at the gas-diffusion layer/bipolar plate interface)

Nafion and Pt with the surface that is not equally accessible. Moreover, one must understand the difference between the *low* and *high* characteristic bulk current densities and the *thin* and *thick* active layers of cathodes.

Model experiments are carried out in liquid electrolyte solutions. Here, the recorded currents and the solution conductivity are high; hence, the catalytic layers remain virtually unheated. The layers are thin, their internal surface is equally accessible; hence, the Tafel plot slopes, 60 and 120 mV, coincide with those observed in experiments on smooth Pt.

A different situation is observed for fuel cell cathodes. Here, the unequal accessibility of the active layer to the current generation process leads to Tafel slopes of 60 and 240 mV even in the absence of cathode active mass heating. Moreover, for very thin active layers (several μm), it can be assumed that the first Tafel slope (high potential range) extends to the low potential range. Moreover, if in addition to this, the heat conductivity of the heat-removing gas-diffusion layer is insufficiently high and the latter fails to remove heat, then the active layer is inevitably heated. This further extends the potential range with the Tafel slope ~ 60 mV up to values $E \sim 0.6$ V.

REFERENCES

1. Damjanovic, A., Genshaw, M.A., and Bockris, J.O., `M, *J. Phys. Chem.*, 1996, vol. 45, p. 4057.
2. Appleby, A.J., *J. Electrochem. Soc.,* 1970, vol. 117 P, p. 328.
3. Sepa, D.B., Vojnovic, V., and Damjanovic, A., *Electrochim. Acta*, 1981, vol. 26, p. 781.
4. Parthasarathy, A., Martin, C.R., and Srinivasan, S., *J. Electrochem. Soc.*, 1991, vol. 138, p. 916.
5. Zinola, C.F., Luna, A.M., and Arvia, A.J., *Electrochim. Acta*, 1994, vol. 39, p. 1951.
6. Grgur, B.N., Markovic, N.M., and Ross, P.N., *Can. J. Chem.*, 1997, vol. 75, p. 1465.
7. Paulus, U.A., Schmidt, T.J., Gasteiger, H.A., and Behm, R.J., *J. Electrochem. Soc.*, 2001, vol. 495, p. 134.
8. Antoine, O., Bultel, Y., and Durand, R., *J. Electroanal. Chem.*, 2001, vol. 499, p. 85.
9. Paulus, U.A., Wokaun, A., Scherer, G.G., Schmidt, T.J., Stamenkovic, V., Radmilovic, V., Markovic, N.M., and Ross P.N., *J. Phys. Chem. B*, 2002, vol. 106 P, p. 4181.
10. Murthi, V.S., Urian, R.C., and Mukerjee, S., *J. Phys. Chem. B*, 2004, vol. 108, p. 11011.
11. Wakabayashi, N., Takeichi, M., Uchida, H., and Watanabe, M., *J. Phys. Chem. B*, 2005, vol. 109 P, p. 5836.
12. Neyerlin, K.C., Gu, W., Jorne, J., and Gasteiger, H.A., *J. Electrochem. Soc.*, 2006, vol. 153, p. A1955.
13. Mukerjee, S., Srinivasan, S., and Appleby, A.J., *Electrochim. Acta*, 1993, vol. 38, p. 1661.
14. Wang, X., Hsing, I.-M., and Yue, P.L., *J. Power Sources*, 2001, vol. 96, p. 282.
15. Gasteiger, H.A., Gu, W., Makharia, R., Mathias, M.F., and Sompalli, B., in *Handbook of Fuel Cells – Fundamentals, Technology and Applications, V. 3*, Vielstich, W., Lamm, A., and Gasteiger, H., Eds., 2003, Chichester, UK: Wiley, p. 593.
16. Thompsett, D., in *Handbook of Fuel Cells – Fundamentals, Technology and Applications, V. 3*, Vielstich, W., Lamm, A., and Gasteiger, H., Eds., 2003, Chichester, UK: Wiley, p. 467.
17. Gasteiger, H.A., Panels, J.E., and Yan, S.G., *J. Power Sources*, 2004, vol. 127, p. 162.
18. Gasteiger, H.A., Kocha, S.S., Sompalli, B., and Wagner, F.T., *Applied Catalysis B: Environmental*, 2005, vol. 56, p. 9.
19. Chirkov, Yu.G. and Rostokin, V.I., *Elektrokhimiya,* 2004, vol. 40, p. 1036; 2005, vol. 41, p. 1109; 2006, vol. 42, p. 799; 2007, vol. 43, p. 827.
20. Chirkov, Yu.G. and Rostokin, V.I., *Elektrokhimiya*, 2006, vol. 42, p. 806.
21. Chirkov, Yu.G. and Rostokin, V.I., *Elektrokhimiya*, 2009, vol. 45, p. 193.
22. Chirkov, Yu.G. and Rostokin, V.I., *Elektrokhimiya*, 2008, vol. 44, p. 1321.
23. Costamagna, P. and Srinivasan, S., *J. Power Sources*, 2001, vol. 102, pp. 242, 253.
24. Kocha, S.S., in *Handbook of Fuel Cells – Fundamentals, Technology and Applications. V. 3*, Vielstich, W., Lamm, A., and Gasteiger, H., Eds., 2003, Chichester, UK: Wiley, p. 538.
25. Gasteiger, H., Gu, W., Makharia, R., Mathias, M.F., and Sompalli, B., in *Handbook of Fuel Cells – Fundamentals, Technology and Applications. V. 3*, Vielstich, W., Lamm, A., and Gasteiger, H., Eds., 2003, Chichester, UK: Wiley, p. 593.
26. Parthasarathy, A., Srinivasan, S., Appleby, A.J., and Martin, C.R., *J. Electrochem. Soc.*, 1992, vol. 139 P, p. 2530.
27. Mitsushima, S., Araki, N., Kamiya, N., and Ota, K., *J. Electrochem. Soc.*, 2002, vol. 149, p. A1371.
28. Fuller, T. and Newman, J., *J. Electrochem. Soc.*, 1993, vol. 140, p. 1218.
29. Nguyen, T. and White, R., *J. Electrochem. Soc.*, 1993, vol. 140, p. 2178.
30. Ju, H., Meng, H., and Wang, C.-Y., *Int. J. Heat Mass Transfer*, 2005, vol. 48 P, p. 1303.
31. Ramousse, J., Deseure, J., Lottin, O., Didierjean, S., and Maillet, D., *J. Power Sources*, 2005, vol. 145, p. 416.
32. Khandelwal, M. and Mench, M.M., *J. Power Sources*, 2006, vol. 161, p. 1106.
33. Newman, J., in *Electrochemical Systems*, 1991, Eaglewood Cliffs: Prentice Hall, p. 290.
34. Ramousse, J., Didierjean, S., Lottin, O., and Maillet, D., *Int. J. Thermal Sciences*, 2008, vol. 47, p. 1.
35. Vie, J.S.P. and Kjelstrup, S., *Electrochim. Acta*, 2004, vol. 49, p. 1069.
36. Shimpalee, S., Beuscher, U., and Van Zee, J.W., *Electrochim. Acta*, 2007, vol. 52, p. 6748.
37. Chirkov, Yu.G. and Rostokin, V.I., *Elektrokhimiya,* 2007, vol. 43, p. 827.